Evaluation of Input-shaping Control Robustness for the Reduction of Torsional Vibrations

Constanza Ahumada, *Member, IEEE*, Patrick Wheeler, *Fellow, IEEE*

Abstract— **Aircraft drivetrains connect the engine to the electrical power system. In most cases, the drivetrains are relatively flexible and have vibration modes with values below 100 Hz to reduce weight and size. Therefore, electrical loads' connection and disconnection may excite torsional vibrations in the machine's shaft, reducing the drivetrains' lifespan. This interaction is known as electromechanical interaction. This issue can be mitigated using an input-shaping strategy, which reduces the excitation of torsional vibrations by connecting the electrical loads following a pattern, dependent on the drivetrain's natural frequencies. However, since this method is based on the knowledge of the vibration modes attributes, it can be susceptible to parameter's uncertainty. In this paper, a pulsating input shaping method's robustness is assessed, analysing simulation and experimental results. The effect of the inductances is analysed, and a strategy to reduce its effect is proposed. Furthermore, the effect of uncertainty in the mechanical parameters is evaluated, and theoretical analysis is carried out to establish safe operating limits. The theoretical analysis is experimentally validated.**

Keywords— *Aircraft Power System, Electromechanical effects, Load Management, Robustness, Vibration Control.*

I. INTRODUCTION

The More-Electric Aircraft (MEA), in which traditional pneumatical and hydraulic loads are electrically fed, has become a significant trend for future aircraft [1]. MEA electrical loads are often high-power transient or pulsating loads such as the wing ice protection system, environmental control system and engine starting system [2]. The aircraft engine is connected through a drivetrain to an electrical generator which supplies the electrical power system (EPS). One of the main issues with this configuration is that, since the generator shaft is designed to be flexible to reduce its weight, the high-power transient or pulsating loads connection can cause mechanical vibrations in the system.

The increased level of coupling between the EPS and the aircraft drivetrain excites torsional vibrations on the drivetrain shaft [3], [4], which can ultimately damage the drivetrain [5]. Electromechanical interaction in aircraft applications has been analysed in [3], [4], [6]. These studies identified the mechanical vibrations modes, presented models for the study of electromechanical interaction, and demonstrated the excitation of torsional vibrations after electrical loads have been connected. To reduce the electromechanical interaction due to the connection of electrical loads, three approaches usually are taken: In the first, the system can be designed to have higher

damping or stiffness and hence move the mechanical frequencies to safe operating areas and damped the vibrations [7], [8]. However, these methods make the system heavier and larger, which is not desired in aircraft applications [3], [9]. In the second, for systems with periodic excitation, such as a generic drive system, the drivetrain's natural frequencies and vibration modes are first identified [3], [10]. Then the excitation of torsional vibrations is avoided by operating the system at different frequency values.

The third approach aims to reduce the vibrations excited by the non-periodic loads by controlling the machine's torque and speed. In [6], [7], [11], the speed control of the machine, using ramp speed control, is proposed. While this solution is straightforward, it slows down the system dynamics since the optimal slope is not studied. Other strategies propose the use of closed-loop torque controllers using PI [12]–[14], non-linear controllers [15], and adaptive and predictive control [16]. An alternative is the use of anti-resonant filters [12], [17]–[20] that cancel the excitation of torsional vibrations. In this group, input-shaping or Posicast compensator can be found [21]. This compensator shapes the connection of torque to avoid the excitation of the frequencies responsible for the vibrations. Furthermore, it operates in a time lower than half the torsional frequency period, making it much faster than the other methods commonly used.

An input-shaping strategy was tested to reduce electromechanical interactions for aircraft applications in [22], [23]. Contrary to traditional strategies which apply the control on the machine drives, the input-shaping strategy presented in [22], [23] is applied in the electrical load connection. The strategy, called Single Level Multi-edge Switching Loading (SLME), connects electrical loads following a pulsating pattern to reduce torsional vibrations' excitation. However, input-shaping strategies depend on mechanical vibration modes. Additionally, the SLME pulsating load connection is designed to apply squared waveforms torque changes in the aircraft drivetrain, which is not realistic in a system with inductances and capacitances. Thus, the robustness of the method must be assessed.

This paper aims to identify sources of uncertainty for the SLME input-shaping strategy presented in [22], [23], analyse its robustness to parameters uncertainty, and propose strategies that allow increasing the robustness of the method. The contributions of this paper are:

- SLME based input-shaping strategies which reduce the excitation of torsional vibrations with consideration of the inductance of the system.

- A robust analysis of the input-shaping strategies, which study the effect of inductance and uncertainty of frequency and damping in reducing torsional vibrations.
- Experimental validation of the robustness of the SLME input-shaping strategy for the reduction of torsional vibrations.

The rest of the paper is organised as follows: First, the electromechanical system is modelled. In Section III, the proposed input-shaping strategies are introduced. In Section IV, simulation results are presented. In Section V, the robustness of the strategies to frequency, damping and inductance uncertainty is analysed. In Section VI, the system is experimentally validated, and finally, in Section VII, the conclusions are given.

II. MODELLING OF THE ELECTROMECHANICAL SYSTEM

An electromechanical interaction model with torsional vibration features similar to those of an aero-engine was presented in [4]. As shown in Fig. 1, the model includes a drivetrain (shafts and gearbox), generator and electrical loads. The mechanical and electrical systems are described in the following two subsections.
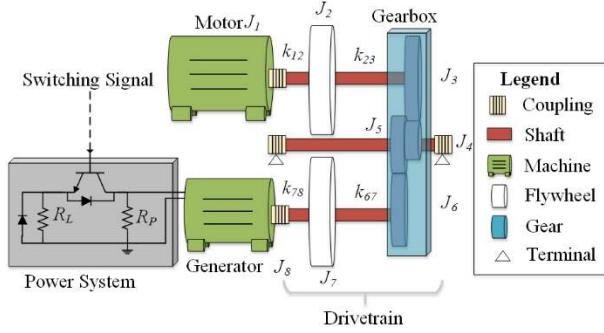

Fig. 1. Electromechanical interaction system under study.

A. Mechanical system modelling

In aircraft applications, temperature and pressure do not affect the lower frequency torsional vibration modes, which are the important ones in terms of electromechanical interaction. Hence, the drivetrain is modelled as a linear lumped mass system, describing loads, shafts, and the gearbox in terms of inertias, stiffness and damping. The drivetrain consists of three shafts rotating at different speeds, one connected to the prime mover, a middle shaft rotating faster, used for experiments out of the scope of this paper, and one to the generator as shown in Fig. 1. The speed ratio between the three shafts is 1:3:1.5, with the motor shaft the slowest. Two flywheels are added to obtain a flexible shaft with natural frequencies below 100 Hz.

The lumped mass model of this system can be described using the following equations

$$J_i\ddot{\theta}_i = T_{(i-1),i} - T_{i,(i+1)} \qquad (1)$$

$$T_{i,(i+1)} = k_{i,(i+1)}(\theta_i - \theta_{i+1}) + d_{i,(i+1)}(\dot{\theta}_i - \dot{\theta}_{i+1}) \qquad (2)$$

where the machines, gears, and flywheels are represented by inertia J_i, while the couplings and shaft are characterised by stiffness $k_{i,i+1}$ and damping $d_{i,i+1}$ between inertias i and $i+$

1. θ_i, $\dot{\theta}_i$, $\ddot{\theta}_i$ model the angle, speed, and acceleration of the inertia i, and $T_{i-1,i}$ and $T_{i,i+1}$ the torque applied to and transmitted by inertia i respectively. Index i varies to model each part of the system, as referred to in Fig. 1. The complete lumped mass system is obtained by evaluatting (1) and (2) for the eight inertias representing the machines, flywheels, and gears, as shown next

$$J\ddot{x} + D\dot{x} + Kx = f(t)$$

$$x = \begin{bmatrix} \theta_1 \\ \theta_2 \\ \theta_6 \\ \theta_7 \\ \theta_8 \end{bmatrix}, f(t) = \begin{bmatrix} T_m \\ 0 \\ 0 \\ 0 \\ -T_e \end{bmatrix}, J = \begin{bmatrix} J_1 & 0 & 0 & 0 & 0 \\ 0 & J_2 & 0 & 0 & 0 \\ 0 & 0 & J_{3,4,5,6} & 0 & 0 \\ 0 & 0 & 0 & J_7 & 0 \\ 0 & 0 & 0 & 0 & J_8 \end{bmatrix}$$

$$D = \begin{bmatrix} d_{12} & -d_{12} & 0 & 0 & 0 \\ -d_{12} & d_{12}+d_{23} & -d_{23} & 0 & 0 \\ 0 & -d_{23} & d_{23}+d_{67} & -d_{67} & 0 \\ 0 & 0 & -d_{67} & d_{67}+d_{78} & -d_{78} \\ 0 & 0 & 0 & -d_{78} & d_{78} \end{bmatrix} \qquad (3)$$

$$K = \begin{bmatrix} k_{12} & -k_{12} & 0 & 0 & 0 \\ -k_{12} & k_{12}+k_{23} & -k_{23} & 0 & 0 \\ 0 & -k_{23} & k_{23}+k_{67} & -k_{67} & 0 \\ 0 & 0 & -k_{67} & k_{67}+k_{78} & -k_{78} \\ 0 & 0 & 0 & -k_{78} & k_{78} \end{bmatrix}$$

where J is the inertia matrix referred to the generator, D is the damping matrix referred to the generator, K is the stiffness matrix referred to the generator; x is the state of each element in the system, and $f(t)$ is the torque applied.

The drivetrain interacts with the engine and the EPS through the torque applied by the engine $T_1 = T_m$ and the torque applied to the generator $T_8 = T_g$.

B. Electrical system modelling

As shown in Fig. 1, the EPS is modelled as a DC system since, for the mechanical drivetrain, the torque applied by an AC or DC system are equivalent. The generator is a DC machine with an independent winding connection, operating with constant field current (i_f), which operation is described by

$$T_e(t) = k i_f i_a(t) \qquad (4)$$

$$E(t) = R_a i_a(t) + L_a \frac{di_a(t)}{dt} + v_a(t) \qquad (5)$$

$$v_a(t) = R_{eq}(t) i_a(t) \qquad (6)$$

$$E(t) = k i_f \dot{\theta}_8(t) \qquad (7)$$

with k the rotational inductance, i_f the field current, $i_a(t)$ the armature current, $E(t)$ the back-EMF, $v_a(t)$ the armature voltage, R_a and L_a the armature resistance and inductance, respectively, $\dot{\theta}_8(t)$ is the generator speed, and $R_{eq}(t)$ is the total load connected to the system. The total load connected to the system $R_{eq}(t)$ is controlled by an insulated-gate bipolar transistor (IGBT), which can connect/disconnect the load. The torque applied to the mechanical system T_g is given by

$$T_g = T_e - T_w \qquad (8)$$

where T_e is the torque producing the electromotive force and T_w the torque consumed by the windage. When the torque consumed by the windage is much smaller than the one applied to the mechanical system, T_g can be approximated as $T_g \approx T_e = k i_f i_a(t)$. Therefore, the torque applied to the drivetrain is proportional to the load connected, and by controlling the IGBT, the excitation of torsional vibrations can be reduced.

III. PROPOSED INPUT-SHAPING STRATEGIES

In this section, the two input-shaping strategies that can be applied to systems with inductance are presented. Firstly, a pulsating input shaping strategy, which does not consider the system's inductance, is presented. Then, two strategies that allow the application of the pulsating input shaping strategy to inductive systems are proposed. Finally, the solutions obtained with the three algorithms are compared.

A. Single Level Multi-edge Switching Loading (SLME) method

For a linear time-invariant system, the response to an external excitation can be modelled following the modal approach [5]. Each step will excite the n vibration modes of the system, which are modeled as a function of its natural frequency. Modelling the excitation as a series of steps p_k at times T_k (in [s]) with $k \in [1 \dots m]$, the response of the system is given by

$$x(t) = h_0 p_0 + \sum_{j=1}^{n} \left[2h_{jr} \sum_{k=1}^{m} p_k e^{-\xi_j \omega_{nj}(t-T_k)} \cos\left(\omega_{dj}(t-T_k)\right) \right. \\ \left. + 2h_{jc} \sum_{k=1}^{m} p_k e^{-\xi_j \omega_{nj}(t-T_k)} \sin\left(\omega_{dj}(t-T_k)\right) \right] \quad (9)$$

In this equation, ω_{nj} is the j natural frequency in rad/s and ξ_j the associated damping, while ω_{dj} is the damped frequency, modelled as $\omega_{dj} = \omega_{nj}\sqrt{1-\xi_j^2}$. h_{jr} and h_{jc} are the real and imaginary components of the step response. Finally, $h_0 p_0$ is the constant term obtained from the rigid mode of the system with $\omega_{n0} = 0$.

The vibrations produced by the torsional modes $j \in [1 \dots m]$ associated with the natural frequency ω_{nj} are zero when the set of steps is orthogonal to the vibration mode. This condition is met when the following equation is satisfied.

$$\left. \begin{array}{l} \sum_{k=1}^{m} p_k e^{-\xi_j \omega_{nj} T_k} \cos\left(\omega_{dj} T_k\right) = 0 \\ \sum_{k=1}^{m} p_k e^{-\xi_j \omega_{nj} T_k} \sin\left(\omega_{dj} T_k\right) = 0 \end{array} \right\} \forall \omega_{nj}, \xi_j \quad (10)$$

Therefore, finding the step p_k and the connection time T_k that solve (10), the excitation of vibrations after the steps have been applied can be eliminated. The concept of modelling a load applied as a desired output function is known as input-shaping [21].

In [22] was proposed that neglecting the inductance of the system, the mechanical torque is proportional to the resistive load connected, since, as shown in (4), $T_g \approx T_e$ is proportional to the armature current i_a. Therefore, controlling the electrical load switching, the total torque applied can be controlled, as

pulsating steps of values $p_k = (-1)^{k+1}$ at times T_k. The number of steps for a system with n frequencies is given by $m = 2n + 1$. Replacing the values of p_k into (10), and expanding for n natural frequencies, the following system can be derived

$$\begin{bmatrix} \sum_{k=1}^{m} (-1)^{k+1} e^{-\xi_1 \omega_{n1} T_k} \cos(\omega_{d1} T_k) \\ \sum_{k=1}^{m} (-1)^{k+1} e^{-\xi_1 \omega_{n1} T_k} \sin(\omega_{d1} T_k) \\ \vdots \\ \sum_{k=1}^{m} (-1)^{k+1} e^{-\xi_n \omega_{nn} T_k} \cos(\omega_{dn} T_k) \\ \sum_{k=1}^{m} (-1)^{k+1} e^{-\xi_n \omega_{nn} T_k} \sin(\omega_{dn} T_k) \end{bmatrix} = 0 \quad (11)$$

The load connection times T_k are found solving the non-linear system of (11), considering $T_1 \leq T_2 \leq \cdots \leq T_k \leq \cdots \leq T_m$ and $T_1 = 0$. Since the system obtained is non-linear, it is solved using numerical optimisation. This strategy was called in [22] Single Level Multi-edge Switching Loading (SLME). It can be applied to aircraft applications, where electromechanical or solid-state switches are used to connect electrical loads. Fig. 2 shows the expected response of a system when the input-shaping strategy is applied. In Fig. 2 (a), the load is connected as one step, while in Fig. 2 (b), the open-loop input-shaping strategy is applied, and, consequently, torsional vibrations are not excited.
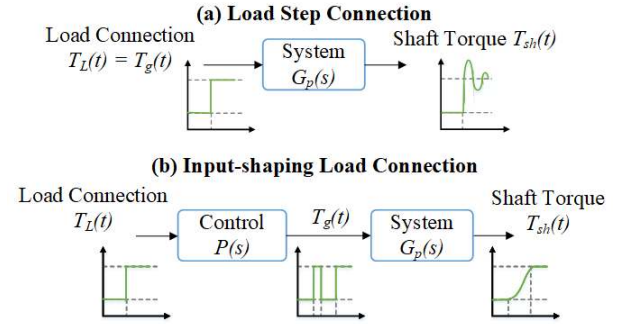

Fig. 2. System diagram with and without the input-shaping strategy.

Since this solution considers no inductance in the system, this paper introduces two new strategies that include inductance, which are presented next.

B. Proposed Single Level Multi-edge Switching Loading with Inductance (SLME-I)

As mentioned, the SLME strategy does not consider the inductances in the system. Since the torque applied to the mechanical system is given by (4) when the system presents an inductive behaviour, the armature current is not square, and thus, neither is the torque. Therefore, in an inductive system, the SLME strategy does not eliminate the excitation of torsional vibrations after the pulsating load has been applied. Two modified SLME strategies are proposed to connect the electrical loads following a switching pattern considering the inductance.

The first one, called SLME-I1, consists of modelling the load connection p_k of the equation system of (10) by their actual shape instead of squared waveforms. For this reason, the load connection p_k is modelled as the sum of infinite steps p_{kt} in time T_k as given by

$$p_k = \sum_{t_p=0}^{T_{k+1}} p_{kt}(t_p) \tag{12}$$

The value of each step p_{kt} is given by

$$p_{kt} = (-1)^k + (-1)^{k+1}\exp(-t_p/\tau_k) - p_{k(t-1)} \tag{13}$$

in which t_p is the time of the step p_{kt}, $\tau_k = L_a/(R_a + R_{eq})$ is the time constant of the EPS, and $p_{k(t-1)}$ is the value of the step in the previous instant. Then, replacing it into the equation system of (10), the following system model can be obtained.

$$\begin{bmatrix} \sum_{k=1}^{m}\sum_{t_p=0}^{T_{k+1}} p_{kt}e^{-\xi_1\omega_{n1}(T_k+t_p)}\cos\left(\omega_{d1}(T_k+t_p)\right) \\ \sum_{k=1}^{m}\sum_{t_p=0}^{T_{k+1}} p_{kt}e^{-\xi_1\omega_{n1}(T_k+t_p)}\sin\left(\omega_{d1}(T_k+t_p)\right) \\ \vdots \\ \sum_{k=1}^{m}\sum_{t_p=0}^{T_{k+1}} p_{kt}e^{-\xi_n\omega_{nn}(T_k+t_p)}\cos\left(\omega_{dn}(T_k+t_p)\right) \\ \sum_{k=1}^{m}\sum_{t_p=0}^{T_{k+1}} p_{kt}e^{-\xi_n\omega_{nn}(T_k+t_p)}\sin\left(\omega_{dn}(T_k+t_p)\right) \end{bmatrix} = 0 \tag{14}$$

Solving (14), the electrical load connection times T_k can be obtained.

When working with a high number of natural frequencies, the non-linear equation system of (14) can take a high time to converge. An alternative to the exact model of the inductance effect is presented in the strategy SLME-I2. This strategy consists of assuming that the load connections are square as in the SLME strategy but adding a delay τ_k to the connection time T_k of the kth step. The delay is given by the inductance time constant $\tau_k = L_a/(R_a + R_{eq})$. Then, the load connection times T_k are found solving the following system

$$\begin{bmatrix} \sum_{k=1}^{m}(-1)^{k+1}e^{-\xi_1\omega_{n1}(T_k+\tau_k)}\cos\left(\omega_{d1}(T_k+\tau_k)\right) \\ \sum_{k=1}^{m}(-1)^{k+1}e^{-\xi_1\omega_{n1}(T_k+\tau_k)}\sin\left(\omega_{d1}(T_k+\tau_k)\right) \\ \vdots \\ \sum_{k=1}^{m}(-1)^{k+1}e^{-\xi_n\omega_{nn}(T_k+\tau_k)}\cos\left(\omega_{dn}(T_k+\tau_k)\right) \\ \sum_{k=1}^{m}(-1)^{k+1}e^{-\xi_n\omega_{nn}(T_k+\tau_k)}\sin\left(\omega_{dn}(T_k+\tau_k)\right) \end{bmatrix} = 0 \tag{15}$$

Next, the solutions of equation systems (11), (14), and (15) are analysed for a two natural frequency system to study the results given by the three SLME strategies.

C. Input-shaping solutions

To compare the three pulsating loads input-shaping strategies SLME, SLME-I1, and SLME-I2, the connection times T_k obtained in each case are going to be analysed. For this, the contour curves at zero of the sine and cosine equations are found for a one frequency system and the EPS presented in section II.

The solution for a one frequency system consists of a 3-step pulse. Since the delays introduced by the inductance depend on the total load R_{eq} connected to the system, the delay time constant has different values for the odd and even pulses. For the system in study, the values obtained are $\tau_1 = \tau_3 = 0.0003\ s$ and $\tau_2 = 0.0022\ s$. Considering the connection time of the first step as $T_1 = 0$, connection times T_2 and T_3 must be found. Fig. 3 shows the results obtained for the three strategies when the damping of the mechanical system is $\xi = 0$ and $\xi = 0.1$ respectively. Fig. 3 (a) and (b) show the results obtained for the SLME strategy, Fig. 3 (c) and (d) for the SLME-I1 strategy, and Fig. 3 (e) and (f) for the SLME-I2 strategy. The curves show all the values that the sine and cosine equations take as a function of the normalised periods $\Gamma_k = T_k/T_n$, with $T_n = 2\pi/\omega_n$. The intersections of the curves are the solutions of the input-shaping strategies.

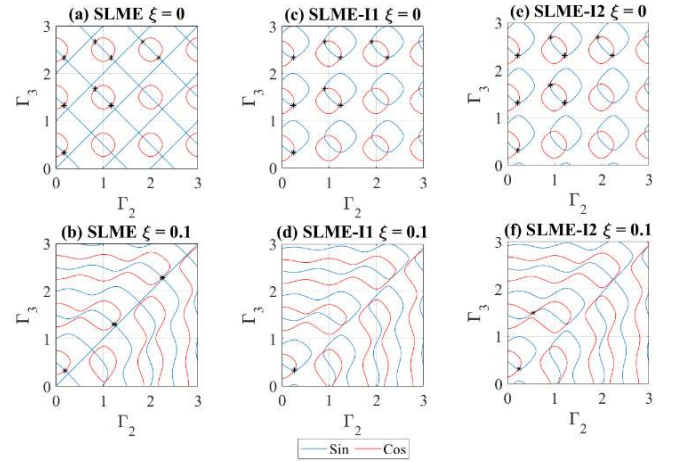Fig. 3. Input-shaping strategy solutions for one ω_n with $\xi = 0$ and $\xi = 0.1$: (a) and (b) SLME, (c) and (d) SLME-I1, (e) and (f) SLME-I2.

Comparing Fig. 3 (a) with (c) and (e), it is observed that the system inductance modifies the sine and cosine curves changing the connection times obtained for SLME, SLME-I1 and SLME-I2 strategies. However, when comparing the curves obtained for the strategies SLME-I1 and SLME-I2, it is observed that they present negligible differences. Therefore, SLME-I1 allows optimal reduction of the vibrations, whereas SLME-I2 allows almost optimal reduction while reducing the computational time compared to SLME-I1. Moreover, the plots obtained for $\xi = 0.1$ show that for a higher damping ratio, the three methods' results converge to the same value, indicating that for a damped system, the input-shaping strategy is more

robust to the effect of the system inductance. Finally, it is worth highlighting that, regardless of the method, there is always a solution inside half a system period.

IV. SIMULATION RESULTS

In this section, the input-shaping control strategies proposed to reduce the excitation of torsional vibrations are applied to the electromechanical system presented in Section II. First, the SLME strategy presented in [22] is tested in a system with and without inductance. After the results obtained with the proposed strategies are shown, and the frequency response is analysed.

The system is modelled in Simulink with the parameters shown in Table I. These values are selected to represent an aircraft system [3], [4] and are referred to the generator side. The torsional vibration modes for which the input-shaping strategies are going to be solved are $f_1 = 36.15$ Hz, $\xi_1 = 0.0127$ and $f_2 = 86.54$ Hz, $\xi_2 = 0.0194$.

TABLE I   PARAMETERS OF THE ELECTRICAL SYSTEM.

Parameter	Value
Armature resistance	$R_a = 4\,\Omega$
Initial load	$R_{eq}(0) = 60\,\Omega$
Final load	$R_{eq}(\infty) = 4.6\,\Omega$
Rotational inductance	$k = 127\,mH$
Armature Inductance	$L_a = 19\,mH$
Referred Motor Inertia	$J_1 = 26\,\text{kg}\cdot\text{cm}^2$
Referred Motor Flywheel Inertia	$J_2 = 170\,\text{kg}\cdot\text{cm}^2$
Gears Inertia	$J_{3+4+5+6} = 150\,\text{kg}\cdot\text{cm}^2$
Generator Flywheel Inertia	$J_7 = 390\,\text{kg}\cdot\text{cm}^2$
Generator Inertia	$J_8 = 5\,\text{kg}\cdot\text{cm}^2$
Referred Motor Coupling Stiffness	$k_{12} = 50.4\,\text{kN}\cdot\text{m/rad}$
Referred Motor Shaft Stiffness	$k_{23} = 0.96\,\text{kN}\cdot\text{m/rad}$
Generator Shaft Stiffness	$k_{67} = 2.2\,\text{kN}\cdot\text{m/rad}$
Generator Coupling Stiffness	$k_{78} = 113\,\text{kN}\cdot\text{m/rad}$

A. Load connection with SLME strategy

The electromechanical system was tested for a load step connection and applying the strategy without and with inductance in the electrical system. The DC generator was fed with a 6.2 A constant field, and the load was connected from 0.37 Nm to 2.97 Nm.

Fig. 4 shows the results obtained for the electromechanical system operating with constant i_f when an electrical load is connected using the proposed method. Fig. 4 (a) and (b) show the uncontrolled step connection, while Fig. 4 (c) and (d) show the results using the SLME strategy in the ideal case of a system without inductance, and Fig. 4 (e) and (f) show the results with the SLME strategy in a system with inductance. Fig. 4 (a), (c), (e) show the armature current and Fig. 4 (b), (d), (f) show the applied torque (T_g in red) and the shaft torque (T_{sh} in blue).

With the SLME strategy, the electrical load is connected as a series of pulses, which timing and amplitude are found by solving (11). The results show that the step connection of electrical loads excites torsional vibrations (Fig. 4 (b)), while the connection using the SLME strategy eliminates the

vibrations when there is no inductance on the system (Fig. 4 (d)). When the system has inductance, the torque T_g is no longer square, and hence the vibrations are reduced but not eliminated, as shown in Fig. 4 (f).
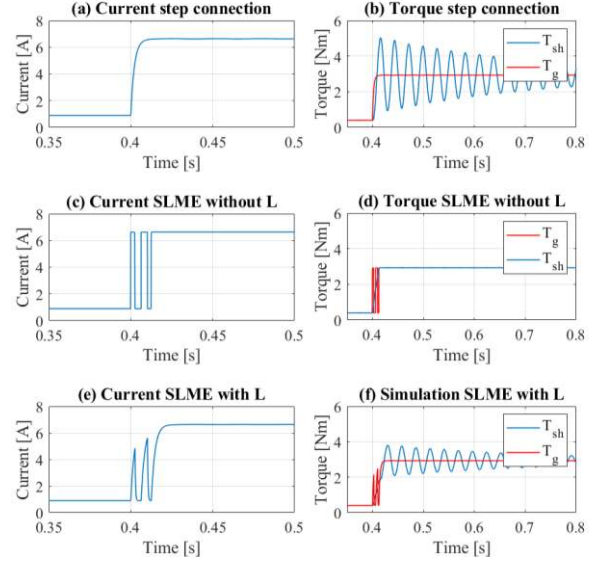

Fig. 4. Torsional vibrations excited by the load connection: (a) and (b) step connection, (c) and (d) SLME connection in a system without inductance, and (e) and (f) SLME connection in a system with inductance.

B. Load connection with proposed SLME strategies

As shown in Fig. 4, when there is inductance, the excited torsional vibrations are reduced but not eliminated by the SLME technique. This result can be improved when the same system is tested using the proposed strategies SLME-I1 and SLME-I2, which are solved considering the system's inductance. Fig. 5 show the results obtained when the load is connected following the connection times obtained, solving (11), (14), (15) for the natural frequencies previously identified.
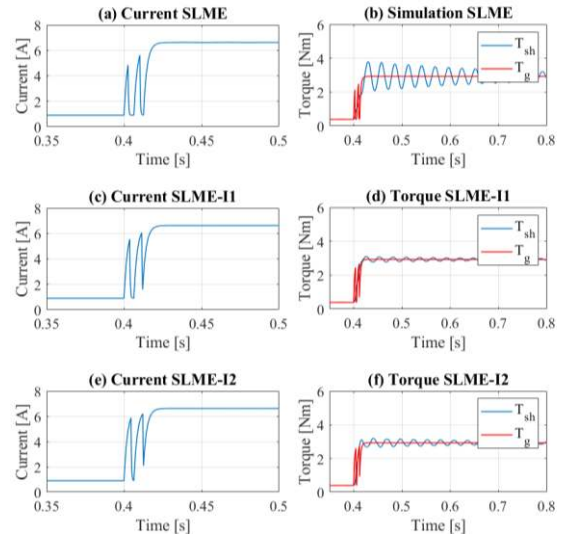

Fig. 5. Torsional vibrations excited by the SLME strategies with inductance: (a) and (b) SLME, (c) and (d) SLME-I1, and (e) and (f) SLME-I2.

Fig. 5 (a) and (b) show the results obtained with the SLME strategy and inductance in the system, while Fig. 5 (c) and (d) show the SLME-I1 connection, and Fig. 5 (e) and (f) show the results with the SLME-I2 strategy. TABLE II presents the overshoot, settling time (to 5% of the steady-state value), and the time taken for the solver to converge in each strategy. It is observed that the methods with inductance in their design SLME-I1 and SLME-I2 lower the excitation of torsional vibrations to values close to zero, reducing the overshoot and the settling time. Moreover, since SLME-I1 models the exact shape of the connection, it allows obtaining better results than SLME-I2, which only adds the delay introduced by the inductance to the step connections. However, the time taken to find the solution with SLME-I1 is 20 times higher than for the SLME-I2 strategy. This difference is heightened in systems with a higher number of vibrations modes to cancel. Also, since the solver requires high accuracy, SLME-I1 does not eliminate the vibrations as was expected.

TABLE II   LOAD CONNECTION PERFORMANCE

Strategy	Solver Time [s]	Overshoot [%]	Settling Time [ms]
Step	0	71.74	876
SLME	0.86	29.75	612
SLME-I1	19.81	6.17	82
SLME-I2	0.61	9.34	196

Despite the remaining vibrations obtained, the results presented by both strategies show that the inductance in a system is not an obstacle to eliminate the vibrations produced by electromechanical interaction. This analysis can be extended to systems with capacitance, showing that the pulsating connection of electrical loads is a feasible solution for reducing the electromechanical interaction.

C. Frequency analysis

The discrete Fourier transform was computed through the FFT of the transient response is analysed to characterise the vibrations modes excited by the connection of the electrical loads with each strategy. Fig. 6 shows the results obtained for a step connection and the connections using the SLME strategy in a system with inductance and with the proposed strategies SLME-I1 and SLME-I2.
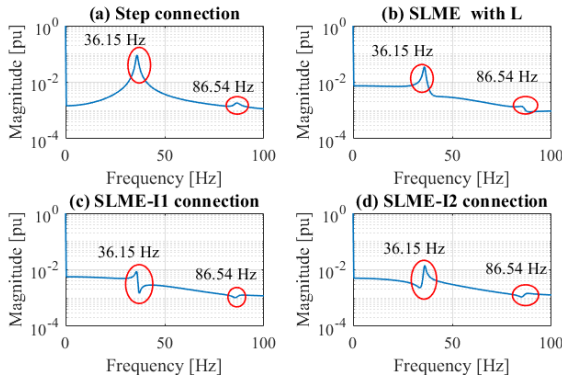

Fig. 6. FFT after the load connection: (a) step response, (b) SLME with inductance, (c) SLME-I1, and (d) SLME-I2

When the frequency spectrums are compared, it can be noted that the step connection excites frequencies, which are reduced when the SLME strategies are applied. Thus, verifying that the use of the proposed input shaping strategies allows the reduction of torsional vibrations after the sequence of pulsed connections has been applied to the system independently of the system's inductances. Next, the robustness of the SLME strategies is studied.

V. ROBUSTNESS ANALYSIS

Theoretical robustness analysis is carried out to establish the operating limits at which the pulsating load input-shaping strategies are beneficial for the electromechanical system. The study analyses the overshoot and settling time of the load connection response under uncertainty of the drivetrain's frequencies and damping and applying the strategies with and without inductance. The overshoot and settling time obtained for a step response in Section IV are taken as a reference to establish an operating range for the strategies.

A. Original SLME robustness to frequency and inductance

The overshoot and settling time of a load connection are analysed for studying the original SLME robustness to frequency and damping ratio uncertainty in the system presented in Section II for the cases with and without inductance in the system. Fig. 7 shows the results obtained when the damping of ω_{n1} and ω_{n2} , named ξ_1 and ξ_2 respectively, are varied from 0 to 0.65 and considered for the connection of loads in the system presented in Section II. The results from Fig. 7 show that, for uncertainty in the damping of the second vibration mode ξ_2 and for values of damping $\xi_1 <$ 0.1, the SLME strategy is not affected. These damping values are consistent with the ones obtained in aircraft applications since higher damping implies an increased weight. Therefore, the SLME strategy is considered robust to damping uncertainty, and from now on, the analysis will focus on frequency uncertainty and the presence of inductance.
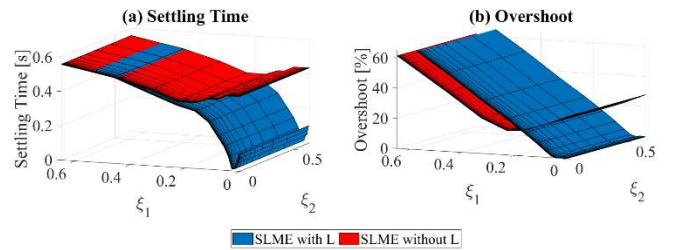

Fig. 7. SLME robustness to damping uncertainty and inductance: (a) settling time, (b) overshoot

Fig. 8 shows when the original SLME strategy is solved for frequencies ω_{n1} and ω_{n2} with ± 50 % of error. The red surface shows the results obtained when the SLME strategy was applied to the ideal case, while the surface in blue shows the results obtained when the SLME connection was used considering the system inductance.
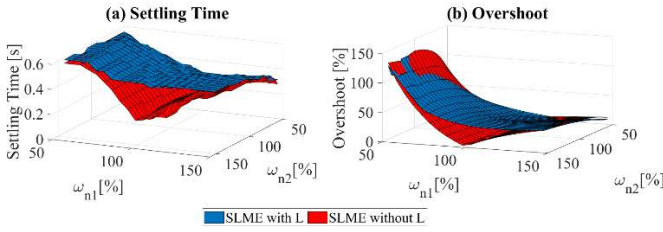
Fig. 8. SLME robustness to frequency uncertainty and inductance: (a) settling time, (b) overshoot

The results from Fig. 8 show that, as with the damping, the uncertainty in the frequency ω_{n2} does not affect considerably the performance of the strategy. However, uncertainty in ω_{n1} can produce overshoot higher than the one obtained with a step connection, and hence safe uncertainty margins for ω_{n1} must be established. From Fig. 8 (b), it is observed that under-measuring the frequency produces higher vibrations than detecting a value higher than the real one. In terms of settling time, the same behaviour of Fig. 8 (b) is obtained for Fig. 8 (a). Moreover, any value of frequency higher than the nominal allows the reduction of the vibrations compared to the step case, making the strategies suitable, even if the frequency is not precisely known. Even more, in a range of $\pm 10\,\%$, the overshoot increase can be considered negligible.

Having established the effect of the damping and frequency uncertainty, the effect of inductance is assessed. It is observed that for damping and frequency values close to the real one, not considering the presence of inductance (red surfaces in Fig. 7 and Fig. 8) in the input-shaping strategy increases the overshoot and settling time. This increase is higher than the one obtained for frequency uncertainty in the $\pm 10\,\%$ range. However, as shown by the simulation results in Section IV, the final settling time and overshoot are still lower than those obtained in a step connection, validating the method's use.

B. Robustness comparison of the pulsating strategies

Having established the effect of inductance, damping and frequencies uncertainty, using the original SLME, SLME-I1, and SLME-I2 techniques, the importance of identifying every frequency and the comparison between the methods are assessed. With this aim, Fig. 9 shows the robustness to frequency uncertainty in a range of $\pm 50\,\%$ of the nominal frequency for the three strategies analysed: SLME without inductance (in blue), SLME-I1 (in red), and SLME-I2 (in yellow). It is observed that the surfaces obtained are similar, showing that the three methods have similar robustness.
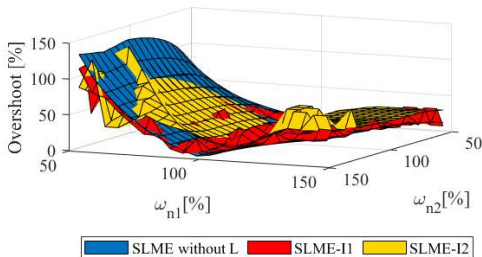

Fig. 9. SLME strategies robustness to frequency uncertainty.

The similar performance of the strategies is verified in Fig. 10, where the robustness to ω_{n1} and ω_{n2} with and without identifying the second frequency is depicted. The results obtained with SLME without inductance are shown in blue, while the SLME-I1 and SLME-I2 results are shown in red and yellow. First, it is observed that for the uncertainty of ω_{n1} with and without identifying ω_{n2} and for ω_{n2} failing to identify ω_{n1}, the curves obtained by the three strategies are similar. However, this is not true in Fig. 10 (b), which shows that uncertainty in ω_{n2} while correctly identifying ω_{n1} affect SLME-I1 and SLME-I2 techniques robustness negatively in comparison with SLME applied to an ideal system. This difference is associated with the smaller pulses obtained for higher frequencies. Since smaller pulses have a higher chance of changing their values when the strategies consider the inductance, the proper identification of higher frequencies is more critical for SLME-I1 and SLME-I2. However, regardless of the strategy, the change in overshoot for uncertainty in ω_{n2} is considerably lower than for uncertainty in ω_{n1}.

When comparing the robustness of the methods when the strategies have been solved for a lower amount of frequencies, as in Fig. 10 (c) and (d), it is observed that failing to identify the lower frequencies affects more the robustness of the method. Still, for frequencies in a $\pm 10\,\%$ range, the nominal frequency generates overshoots lower or equal to the step connection, making SLME, SLME-I1 and SLME-I2 strategies helpful in the reduction of torsional vibrations.
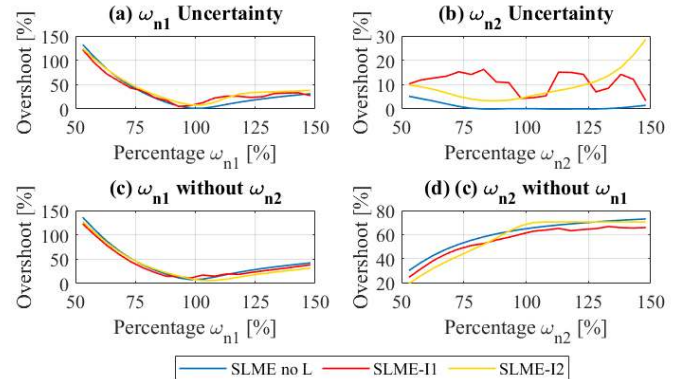

Fig. 10. SLME strategies robustness to frequency number: (a) uncertainty in ω_{n1} with ω_{n2}, (b) uncertainty in ω_{n2} with ω_{n1}, (c) uncertainty in ω_{n1} without ω_{n2}, (d) uncertainty in ω_{n2} without ω_{n1}

Fig. 11 shows the simulation results obtained for four frequency uncertainty cases. In Fig. 11 (a) the original SLME strategy was solved for f_{1n} and f_{n2} with a +10% error, in Fig. 11 (b) the strategy SLME-I2 was solved for f_{1n} and f_{n2} with a +10% error, in Fig. 11 (c) the SLME strategy was solved for f_{n1} with an error of -11% without considering the damping, and in Fig. 11 (d) the SLME strategy was solved for f_{n1} with an error of +12% without considering the damping. These last two connections are equivalent to the solution shown in Fig. 3 (a), which is similar to using a soft starter with a period of 25% of the first natural frequency and 40% of the period of both frequencies. Table III shows the overshoot and settling time obtained in each of the four cases.

The results show that, as observed in Fig. 8 and Fig. 9, the torsional vibrations are reduced when the system has a 10% of uncertainty, and the number of frequencies is correctly identified. However, when the number of frequencies is not correctly identified, and the strategy is solved for only one frequency, the results vibrations excited can be higher than for a single step connection. Since this solution is a uniformly distributed pulse, which is easy to apply in a soft starter, when working with these applications, it is crucial to correctly identify the frequency to avoid exciting higher vibrations, which are detrimental to the mechanical system.
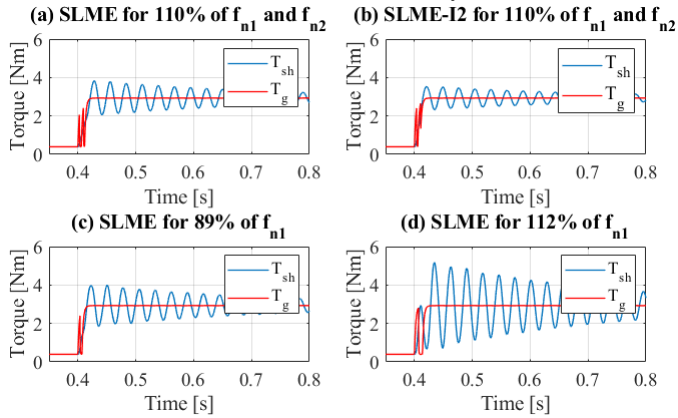

Fig. 11. Torsional vibrations obtained for different pulsating connections in the system with inductance: (a) SLME solved for 110% of f_{n1} and f_{n2}, (b) SLME-I2 solved for 110% of f_{n1} and f_{n2}, (c) SLME solved for 89% of f_{n1}, (d) SLME solved for 112% of f_{n1}

TABLE III
FREQUENCY UNCERTAINTY COMPARISON BY SIMULATION

Frequencies	Overshoot [%]	Settling Time [ms]
110% SLME	30.62	630
110% SLME-I2	18.04	489
89% SLME WITH f_{n1}	35.30	710
112% SLME WITH f_{n1}	76.53	905

In summary, the robust analysis of the strategies has shown that failing to recognise one frequency reduces the robustness of the input-shaping load connections substantially, while failing to include the system's inductance is critical for the technique effectiveness. Moreover, failing to identify the presence of the lower frequency affects the robustness of the SLME strategies considerably more than for frequency f_2. However, for frequencies with 10 % uncertainty, the proposed techniques' results are always better than those obtained with the pure step connection. Since the experimental data's uncertainty is ± 2 Hz, the robustness of the method is considered acceptable.

VI. EXPERIMENTAL RESULTS

Fig. 12 shows the experimental setup, which models the system of Fig. 1. The setup is composed of a 2.2 kW, two pairs of poles induction motor with a nominal speed of 1445 rpm driven using Volt/frequency control while a 1 kW Nidec Universal Motor is operated as an independent field DC generator. A resistance bank of 60 Ω and a variable load resistance composes the EPS. An IGBT, controlled with an Infineon® XE166FN microcontroller, connects and disconnects the load resistance. The mechanical drivetrain is designed to obtain the same resonance frequencies of the simulation test using two flywheels. The system is designed considering the same parameters of the simulation of Table I.
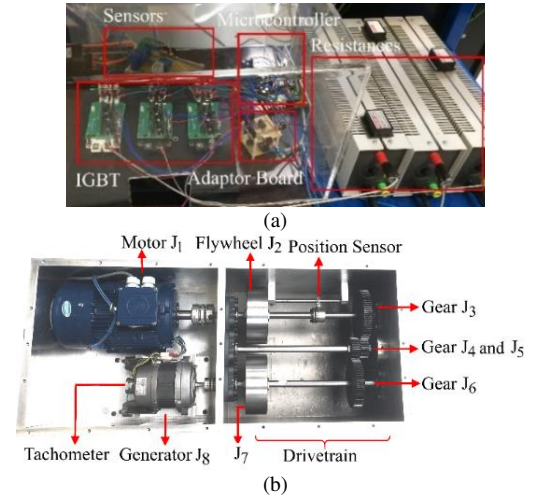

Fig. 12: Experimental setup: (a) electrical system and (b) mechanical system.

The field current, armature current, and armature voltage are obtained using current and voltage transducer sensors model LA100-P and LV25-P, respectively. These sensors are connected to dSpace using an acquisition frequency of 10 kHz. The speed and torque are determined using the sensorless method presented in [4]. This method estimates the torque using a model-based back-EMF strategy, in which the torque in the shaft is calculated from the machine torque T_g and the transient response $T_{transient}$, as shown in the following equation:

$$T_{sh} = T_g + T_{transient} \qquad (16)$$

The machine torque T_g is obtained from the field and armature current measurements, which are replaced in (8). Therefore, the transient component $T_{transient}$ can be given by the following equation:

$$T_{transient} = J_g \ddot{\theta}_8 \qquad (17)$$

Where J_g is the inertia and $\ddot{\theta}_8$ is the machine acceleration, obtained replacing the measured signals (field current and armature current and voltage) in (7) and (8).

As presented in Section III, the proposed input shaping method depends on the drivetrain's frequency and damping. Thus, to validate the mechanical system design, the drivetrain resonance frequencies are verified through the discrete Fourier transform analysis after a step connection is applied to the system. The information recorded consists of 10 seconds of data with a sampling frequency $f_s = 10$ kHz. Fig. 13 shows the normalised Fourier response of the armature current when the field current is 6.2 A, and the system is operating at two speeds. In Fig. 13 (a), the generator speed is 1500 rpm, while in Fig. 13 (b), the generator speed is 2000 rpm.

As shown in Fig. 13, two sets of frequency are identified. In black, the frequencies related to the speed are marked, and in red, the drivetrain's torsional frequencies are highlighted. Since the measurements are taken from the DC generator's armature current, when the speed is 1500 rpm, a peak at 25 Hz is

observed. Instead, when the generator speed is 2000 rpm, a peak at 33 Hz is obtained. The second pair of peaks obtained at 50 Hz and 67 Hz is associated with the middle shaft speed, which rotates at 3000 rpm and 4000 rpm in each case. The peak at 0 Hz represents the rigid mode of the system. Then, the torsional frequencies are the ones found in both tests, and their values are $f_1 = 35.5$ Hz and $f_2 = 77.1$ Hz.
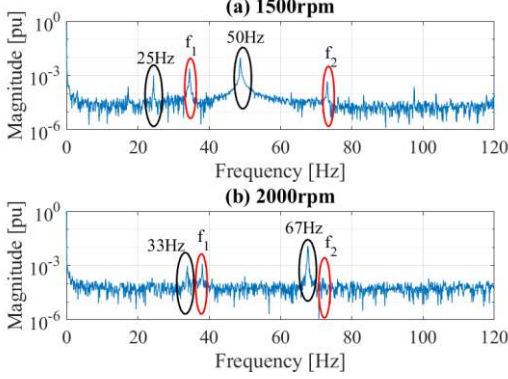

Fig. 13. Fourier analysis after a step connection: (a) speed 1500 rpm, (b) speed 2000rpm.

The Hilbert Transform combined with empirical mode decomposition (EMD) presented in [24], [25], is used to identify the damping ratio. The method consists of separating each vibration mode using EMD. Then, to each mode, the Hilbert Transform is applied. The results obtained are expressed in terms of the amplitude and angle as given by the following equations

$$A(t) = A_0 e^{-\xi \omega_n t} \rightarrow \log(A(t)) = \log(A_0) - \xi \omega_n t \qquad (18)$$

$$\theta(t) = \omega_d t + \theta_0 \rightarrow \omega(t) = \omega_d = \omega_n \sqrt{1 - \xi^2} \qquad (19)$$

Where ξ is damping ratio, $\omega(t)$ is the instantaneous frequency, ω_d and ω_n are the natural damped and natural frequencies, and A_0 and θ_0 are constants. To obtain the damping ratio and its frequency, a logarithm is applied to (18). The slope of this equation is $-\xi \omega_n$. The damped frequency is obtained by differentiating the angle, as shown in equation (19).

The frequencies and damping are $f_1 = 35.5$ Hz, $\xi_1 = 0.018$ and $f_2 = 77.1$ Hz, $\xi_2 = 0.012$. These values present minimal variation with respect to the simulated ones, making the simulation and experimental systems comparable. These differences are mainly related to parasitic parameters and tolerances of the manufactured mechanical system.

The load's connection as a single step and using the proposed input shaping method is verified solving equation system (11) for the identified frequencies and damping. The results obtained with and without the input shaping strategy are shown in Fig. 14. In Fig. 14 (a) and (c), the machine armature current for the step connection and the SLME connection are shown. In Fig. 14 (b) and (d), the torque applied on the drivetrain (in red) and the shaft torque (in blue) for the two connections are presented. The single-step connection of Fig. 14 (b) excites torsional vibrations in the shaft. These vibrations produce a peak torque of 5.2 Nm in the drivetrain shaft, an overshoot of 80.85 % and settling time of 0.643 s. These values are close to the ones obtained by simulation in Section IV Fig. 4: 71.74 % and $t_s =$

0.876. The small discrepancy is clearly explained by the difference between resonance frequencies and damping values of the simulation and experimental model. Therefore, the theoretical analysis is representative of the electromechanical system.

The results obtained applying the SLME input shaping method, shown in Fig. 14 (d), display that the compensator's use reduces the peak torque vibrations from 5.2 Nm to 3.9 Nm. When comparing the experimental and simulation results for the load connection using the SLME strategy, it is observed that the overshoot (33.90 %) is close to the one obtained by simulation when the inductance is not considered (29.75 %).
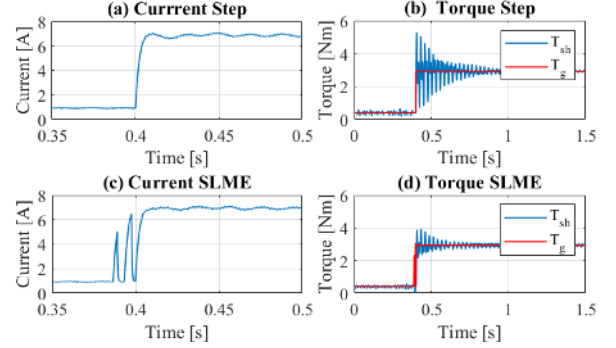

Fig. 14. Load connection experimental results: (a) and (b) current and torque obtained for the step connection, (c) and (d) current and torque obtained using the SLME connection.

Moreover, as described, the frequencies at which (11) was solved present a tolerance. Hence, the calculated connection times may present minor discrepancies from the one currently necessary to suppress the torsional vibrations. Having carried out a theoretical robustness analysis, the experimental system is tested for SLME load connections solved for different frequencies. Three cases are compared: The first case or base case is the results previously presented ($f_{1B} = 35.5$ Hz, $\xi_{1B} = 0.018$, and $f_{2B} = 77.1$ Hz, $\xi_{2B} = 0.012$). The second case is solved for different frequencies f_n and damping ξ ($f_{1C} = 36.4$ Hz , $\xi_{1C} = 0.0219$, and $f_{2C} = 77$ Hz , $\xi_{2C} = 0.0096$). Lastly, to study the importance of the correct identification of the number of torsional frequencies, the system is solved for only one vibration mode f_n ($f_{1B} = 35.5$ Hz, $\xi_{1B} = 0.018$). Fig. 15 shows the results, whereas the overshoot and settling time is presented in Table IV.
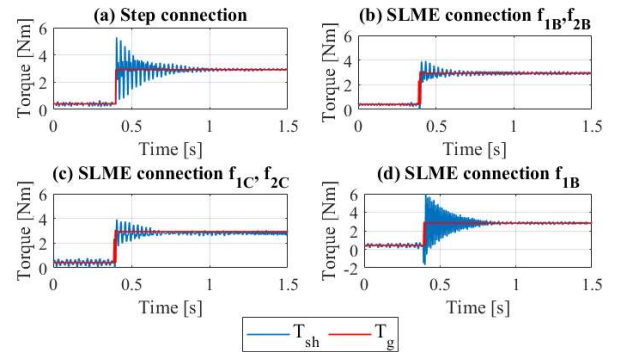

Fig. 15. Experimental robustness of the SLME strategy: (a) step connection, (b) SLME with f_{1B}, f_{2B}, (c) SLME with f_{1C}, f_{2C}, (d) SLME with f_{1B}.

TABLE IV — FREQUENCY UNCERTAINTY COMPARISON

Frequencies	Overshoot [%]	Settling Time [ms]
Step	80.85	643
f_{1B}, f_{2B}	33.90	440
f_{1C}, f_{2C}	38.37	571
f_{1B}	115.41	636

The uncertainty results display that the SLME strategy reduces the overshoot by at least 50 % and the settling time in 100 ms when the number of frequencies is correctly identified (cases f_{1B}, f_{2B} and f_{1C}, f_{2C}) independently of inductance, which allows extending the mechanical components' lifespan by reducing the peak torque and reducing the vibration time. These results are consistent with the theoretical results obtained in Section V. Instead, the results obtained when only one frequency is identified, shown in Fig. 15 (d), display that the torsional vibrations are higher than for the step connection case. Since the theoretical analysis displayed that the correct identification of the number of frequencies does not excite overshoot higher than 100 % for ± 2 % uncertainty as the results have shown for this case, the correct identification of the inductance and its associated delays, which increases the overshoot, becomes essential.

Since the simulation results with inductance and the experimental ones are similar, the SLME strategy has been validated. Furthermore, regardless of the presence of inductance and the uncertainty in the calculated frequencies, the experimental results show that the proposed methodology can reduce the excited torsional vibrations.

Thus, regardless of the system's inductance and uncertainty, the proposed input-shaping strategy can reduce the torsional vibrations excited by the connection of electrical load.

VII. CONCLUSIONS

This paper studied the robustness of a pulsating input-shaping strategy to reduce the excited torsional vibrations by the EPS in an aircraft's drivetrain. Simulation and experimental results have shown that the proposed method effectively allows the reduction of the excited torsional vibrations by the connection of electrical loads by up to 50 % with respect to a single step load connection when the system inductances are not considered and for up to 90 % when they are. The results obtained allow drawing the following conclusions:

- SLME reduces its performance when the system inductance is considered. However, in this situation, the SLME-I1 and SLME-I2 techniques can be considered.
- SLME, SLME-I1, SLME-I2 are robust to damping uncertainty, and for values below $\xi = 0.1$ the method is not affected. Frequency uncertainty of ± 10 % allows the reduction of the vibrations from 79 % to below 20 % of overshoot. For this reason, the method is considered robust for frequencies with uncertainty in this range.
- SLME-I1 and SLME-I2 are equally robust, and while SLME-I2 has a lower torsional vibration reduction, its solver is faster, making SLME-I2 a better solution for systems with a high number of natural frequencies.
- Experimental sensitivity analysis has shown that it is essential to determine the correct number of frequencies

on the system since otherwise, the compensator's effect can be detrimental.

In conclusion, the proposed input shaping methodology reduces vibrations, allowing extending the lifespan of the mechanical components.

REFERENCES

[1] P. W. Wheeler, J. C. Clare, A. Trentin, and S. Bozhko, 'An overview of the more electrical aircraft', *Proc. Inst. Mech. Eng. Part G J. Aerosp. Eng.*, vol. 227, no. 4, pp. 578–585, Apr. 2013.

[2] B. Sarlioglu and C. T. Morris, 'More Electric Aircraft: Review, Challenges, and Opportunities for Commercial Transport Aircraft', *IEEE Trans. Transp. Electrif.*, vol. 1, no. 1, pp. 54–64, Jun. 2015.

[3] T. Feehally, I. E. Damian, and J. M. Apsley, 'Analysis of Electromechanical Interaction in Aircraft Generator Systems', *IEEE Trans. Ind. Appl.*, vol. 52, no. 5, pp. 4327–4336, Sep. 2016.

[4] C. Ahumada and P. Wheeler, 'Modelling of Reduced Electromechanical Interaction System for Aircraft Applications', *IET Electr. Power Appl.*, vol. 13, no. 7, pp. 1061–1070, May 2019.

[5] M. I. Friswell, J. E. T. Penny, S. D. Garvey, and A. W. Lees, *Dynamics of Rotating Machinery*. Cambridge, United Kingdom: Cambridge University Press, 2015.

[6] G. Moore, 'Electromechanical Interactions in Aerospace Gas Turbines', Ph.D. dissertation, Department of Electrical and Electronic Engineering, University of Nottingham, Nottingham, United Kingdom, 2013.

[7] M. A. Valenzuela, J. M. Bentley, and R. D. Lorenz, 'Evaluation of torsional oscillations in paper machine sections', *IEEE Trans. Ind. Appl.*, vol. 41, no. 2, pp. 15–22, Mar. 2005.

[8] Li Ran, Dawei Xiang, and J. L. Kirtley, 'Analysis of Electromechanical Interactions in a Flywheel System With a Doubly Fed Induction Machine', *IEEE Trans. Ind. Appl.*, vol. 47, no. 3, pp. 1498–1506, May 2011.

[9] I. Erazo-Damian, M. F. Iacchetti, and J. M. Apsley, 'Electromechanical interactions in a doubly fed induction generator drivetrain', *IET Electr. Power Appl.*, vol. 12, no. 8, pp. 1192–1199, Sep. 2018.

[10] M. H. Marzebali, S. H. Kia, H. Henao, G.-A. Capolino, and J. Faiz, 'Planetary Gearbox Torsional Vibration Effects on Wound-Rotor Induction Generator Electrical Signatures', *IEEE Trans. Ind. Appl.*, vol. 52, no. 6, pp. 4770–4780, Nov. 2016.

[11] C. Wang, M. Yang, W. Zheng, J. Long, and D. Xu, 'Vibration Suppression With Shaft Torque Limitation Using Explicit MPC-PI Switching Control in Elastic Drive Systems', *IEEE Trans. Ind. Electron.*, vol. 62, no. 11, pp. 6855–6867, Nov. 2015.

[12] G. Mandic, A. Nasiri, E. Muljadi, and F. Oyague, 'Active torque control for gearbox load reduction in a variable-speed wind turbine', *IEEE Trans. Ind. Appl.*, vol. 48, no. 6, pp. 2424–2432, 2012.

[13] J. K. Kambrath, C. Yoon, J. Mathew, X. Liu, Y. Wang, C. J. Gajanayake, A. K. Gupta, and Y.-J. Yoon, 'Mitigation of Resonance Vibration Effects in Marine Propulsion', *IEEE Trans. Ind. Electron.*, vol. 66, no. 8, pp. 6159–6169, Aug. 2019.

[14] F. Zhang, X. Yang, Y. Ren, L. Feng, W. Chen, and Y. Pei, 'A Hybrid Active Gate Drive for Switching Loss Reduction and Voltage Balancing of Series-Connected IGBTs', *IEEE Trans. Power Electron.*, vol. 32, no. 10, pp. 7469–7481, 2017.

[15] I. U. Khan and R. Dhaouadi, 'Robust Control of Elastic Drives Through Immersion and Invariance', *IEEE Trans. Ind. Electron.*, vol. 62, no. 3, pp. 1572–1580, Mar. 2015.

[16] Y. Wang, Q. Zheng, H. Zhang, and L. Miao, 'Adaptive Control and Predictive Control for Torsional Vibration Suppression in Helicopter/Engine System', *IEEE Access*, vol. 6, pp. 23896–23906, 2018.

[17] M. Yang, C. Wang, D. Xu, W. Zheng, X. Lang, and W. Z. M. Y. Dianguo Xu, 'Shaft Torque Limiting Control Using Shaft Torque Compensator for Two-Inertia Elastic System With Backlash', *IEEE/ASME Trans. Mechatronics*, vol. 21, no. 6, pp. 2902–2911, Dec. 2016.

[18] J. Licari, C. E. Ugalde-Loo, J. B. Ekanayake, and N. Jenkins, 'Damping of Torsional Vibrations in a Variable-Speed Wind

Turbine', *IEEE Trans. Energy Convers.*, vol. 28, no. 1, pp. 172–180, Mar. 2013.

[19] L. Liu and D. Xie, 'Performance comparison of two different filter design approaches for torsional vibration damping in a doubly fed induction generator-based wind turbine', *J. Eng.*, vol. 2015, no. 6, pp. 197–204, Jun. 2015.

[20] K.-S. Ou and K.-S. Chen, 'Developing Electromechanical Coupling Macro Models for Dynamic Responses of MEMS Structures With Command Shaping Techniques', *IEEE Trans. Device Mater. Reliab.*, vol. 16, no. 2, pp. 123–131, Jun. 2016.

[21] T. Singh, *Optimal Reference Shaping for Dynamical Systems*. Buffalo, New York, U.S.A.: CRC Press, 2010.

[22] C. Ahumada, S. Garvey, T. Yang, P. Kulsangcharoen, P. Wheeler, and H. Morvan, 'Minimisation of electromechanical interaction with posicast strategies for more-electric aircraft applications', in *IECON 2016 - 42nd Annual Conference of the IEEE Industrial Electronics Society*, Florence, Italy, 2016, pp. 4423–4428.

[23] C. Ahumada and P. Wheeler, 'Evaluation of Posicast Compensator Robustness for the Reduction of Torsional Vibrations', in *2019 IEEE Energy Conversion Congress and Exposition (ECCE)*, Baltimore, MD, USA, 2019, pp. 5870–5877.

[24] W. Lu, X. Du, J. Ding, and X. Wang, 'Modal parameter identification based on fast fourier transform and Hilbert Huang transform', in *2012 2nd International Conference on Consumer Electronics, Communications and Networks (CECNet)*, Yichang, China, 2012, pp. 2703–2706.

[25] C. B. Smith and N. M. Wereley, 'Transient analysis for damping identification in rotating composite beams with integral damping layers', *Smart Mater. Struct.*, vol. 5, no. 5, pp. 540–550, Oct. 1996.

Constanza Ahumada (Member, IEEE) received the B.Sc. and M.Sc. degrees in electrical engineering from the University of Chile, Santiago, Chile, in 2011 and 2013, respectively and the Ph.D degree in electrical and electronic engineering from the University of Nottingham, Nottingham, U.K. in 2018. From the same year she has been an assistant professor with the Department of Electrical Engineering, University of Chile. Her current research interests include electromechanical interaction and control strategies for the reduction of vibrations in aerospace and marine systems and wind turbines.

Patrick Wheeler (Fellow, IEEE) received the B.Eng. degree (Hons.) and the Ph.D. degree in electrical engineering with a focus on matrix converters from the University of Bristol, Bristol, U.K., in 1990 and 1994, respectively. In 1993, he moved to the University of Nottingham, Nottingham, U.K., where he was a Research Assistant with the Department of Electrical and Electronic Engineering. In 1996, he became a Lecturer at the Power Electronics, Machines and Control Group, University of Nottingham, where he has been a Full Professor since January 2008. He was the Head of the Department of Electrical and Electronic Engineering, University of Nottingham, from 2015 to 2018. He is currently the Head of the Power Electronics, Machines and Control Research Group and the Global Director of the Institute of Aerosapce Technology, University of Nottingham, where he was the Li Dak Sum Chair Professor of Electrical and Aerospace Engineering. He has published over 750 academic publications in leading international conferences and journals.

Dr. Wheeler is a member of the IEEE Power Electronics Society Administrative Committee (PEL's AdCom). He is also the Vice-President for Technical Operations of the IEEE Power Electronics Society (PELS).